Energy Reports 6 (2020) 1876–1887

Contents lists available at ScienceDirect

Energy Reports

journal homepage: www.elsevier.com/locate/egyr

Research paper

Synthetical study on the difference and reason for the pore structure of the No. 3 coal reservoir from the southern Qinshui Basin, China, using mercury intrusion porosimetry, low-temperature N_2 adsorption, low field nuclear magnetic resonance, and nuclear magnetic resonance cryoporometry

Huihu Liu [a,*], Ibrahim Issa Farid [a], Shuxun Sang [b,**], Jianhua Shang [a], Haiyan Wu [c], Hongjie Xu [a], Pingshong Zhang [a], Qimeng Liu [a]

[a] School of Earth and Environment, Anhui University of Science & Technology, Huainan 232001, China
[b] School of Resource and Earth Science, China University of Mining and Technology, Xuzhou 221116, China
[c] School of foreign language, Anhui University of Science & Technology, Huainan 232001, China

ARTICLE INFO

Article history:
Received 9 April 2020
Received in revised form 28 June 2020
Accepted 13 July 2020
Available online 18 July 2020

Keywords:
Pore structure
Long field nuclear magnetic resonance
Nuclear magnetic resonance cryoporometry
Low-temperature N_2 adsorption
Mercury intrusion porosimetry
Southern Qinshui Basin

ABSTRACT

This study aimed to synthetically investigate the pore structure characteristics of coal samples from the southern Qinshui Basin in China, by mercury intrusion porosimetry (MIP), low-temperature N_2 adsorption (LTNA), low field nuclear magnetic resonance (LFNMR), and nuclear magnetic resonance cryoporometry (NMRC) methods and to reveal the reasons for the differences in the pore structures of the coal samples. The results show the multimodality of the pore size distribution (PSD) for the different pore diameters from all the samples using MIP and LFNMR, and the bimodality of the PSD of all the samples using LTNA and NMRC. The peak representation in the micropores and transition pores through MIP is generally consistent with that of LTNA, LFNMR, and NMRC, and the peak representation of the PSD in the micropores through MIP is consistent with that of LFNMR. Owing to the differences in the analysis principles and the calculation models from the different analysis methods applied, clear differences are observed in the total volume of the transition pores and micropores based on MIP, LTNA, LFNMR, and NMRC. The anthracitic samples have better connectivity in terms of the PSD than that of the semianthracitic and low-volatile bituminous samples. As revealed through a synthetic analysis, abundantly disconnected transition pores and micropores, as well as poorly connected micropores, occur in coal, particularly in semianthracite and low-volatile bituminous coal. The difference in the PSD between the different coal samples based on the different analysis methods applied is synthetically controlled based on $R_{o,\ max}$, the mineral content in the coal, and the burial depth of the coal samples.

1. Introduction

The pores in a coal reservoir are considered important channels of coalbed methane (CBM) output (Fu et al., 2017; Liu et al., 2017), and the pore size distribution (PSD) partly determines the flow and permeability properties of both CBM and water (Yao and Liu, 2012; Wang et al., 2017).

Numerous methods are used for measuring the PSD of coal, including mercury intrusion porosimetry (MIP), low-temperature N_2 adsorption (LTNA), and high-resolution electron microscopy, the most commonly used of method require mercury porosimetry and gas adsorption using N_2 as the adsorbate. Mercury intrusion is effective in characterizing the porosity with pore diameters ranging from 2∼50 nm, particularly >7.2 nm; with pore diameters of >50 nm (Clarkson et al., 2013), a structural distortion of the pores may be generated at a lower limit of the pore size (approximately 3 nm) owing to the influences of the compressibility (Gane et al., 2004; Shao et al., 2018). In addition, mercury intrusion may be difficult to achieve because of the destruction of the coal reservoir under high pressure. LTNA has an upper pore diameter limit of approximately 300 nm (Clarkson et al., 2011) and is applicable to micropores (pore diameters of <10 nm) and mesopores (pore diameters ranging from 10∼1000 nm). Furthermore, an overlapping pore size region exists, allowing MIP and

* Correspondence to: School of Earth and Environment, Anhui University of Science & Technology, Taifeng Street No.168, Huainan, 232001, China.
** Corresponding author.
E-mail addresses: xixiinformation@163.com (H.H. Liu), Shuxunsang@163.com (S.X. Sang).

https://doi.org/10.1016/j.egyr.2020.07.011

LTNA to be compared. Although comparisons of MIP and LTNA have largely been conducted regarding the PSD for coal (Clarkson and Bustin, 1999; Mastalerz et al., 2008), few discussions on their application for different types of coal have been reported.

In comparisons of traditional MIP and LTNA, some nondestructive analytical methods such as low field nuclear magnetic resonance (LFNMR) have been proposed to characterize the coal porosity with a pore radius greater than 2 nm. Although LFNMR can be used to measure the PSD of interconnected pores (Yao et al., 2010; Yao and Liu, 2012), it cannot be used to quantitatively analyze the closed pores in coal because the PSD is determined through a T_2 spectrogram, which can be obtained using an inverse calculation of the decrement signature of an echo from a columnar sample under saturated water conditions. Furthermore, nuclear magnetic resonance cryoporometry (NMRC) is a method of measuring the phase transition of the testing liquid in the pores of coal, that is, of the freezing–melting action experienced by the liquid. The principle of NMRC has been described in previous reports (Jackson and McKenna, 1990; Mitchell et al., 2008), and it has been shown that the PSD can be determined based on the relationship between the melting point and the pore volume, which can describe not only the PSD of the interconnected pores but also that of the closed pores for coal (Mitchell et al., 2008; Petrov and Furo, 2009). This method has been applied in unconventional oil and gas reservoirs (Mitchell et al., 2008; Petrov and Furo, 2010; Kondrashova and Valiullin, 2013; Zhao et al., 2017), in which the closed pores can be opened after the coal samples are crushed. Given the discussion, NMRC, unlike LTNA, can be applied at elevated temperatures and pressures and is a nondestructive approach, unlike MIP.

Based on the analysis above, MIP has difficulty revealing the structure of the micropores, LTNA cannot be used to describe the macropores, whereas LFNMR can describe the PSD of almost all types of pores, and NMRC can characterize the PSD for a diameter size ranging from 2∼500 nm. Moreover, MIP, LTNA, and LFNMR can only describe the PSD of the interconnected pores in coal, but cannot quantify the disconnected pores in coal; NMRC can describe not only the interconnected pores in coal but also the disconnected pores in coal. Above all, the different types of PSD methods each have different applicabilities, and thus, how the different results can be synthesized to reveal the PSD of the pores in coal should be determined. Therefore, this paper will analyze the PSD of coal not only in terms of the interconnected pores but also in terms of the disconnected pores and synthetically reveal the reason for the differences in the PSD of coal by the different experimental methods.

The southern Qinshui basin (SQB) is a mature CBM basin. CBM exploration and development has received widespread public concern (Wang et al., 2015; Liu et al., 2018; Song et al., 2018; Luo et al., 2019), and many studies have been conducted on the PSD of the SQB (Li et al., 2017; Zhang and Fu, 2018; Zhang et al., 2018; Xu et al., 2019), with different analysis methods applied to evaluate the PSD. However, as a more substantial problem, comprehensive and systematic research on the differences in the multilevel pore structures, from the nano and microscale to the macroscale, between the different types of coal materials in the SQB is relatively inadequate. Therefore, it is necessary to strengthen the exploration of coal reservoirs and the connected and disconnected pore structures in multiple pore size ranges both comprehensively and systematically. In this study, an integrated approach combining traditional characterization methods such as MIP and LTNA for the PSD using new nondestructive techniques applying LFNMR and NMRC was conducted to accurately describe the differences in the PSD in different types of coal materials from the SQB.

In this study, Hodot's pore structure classification system was employed to analyze the PSD. That is, the pore diameters of the micropores, transition pores, mesopores, and macropores are $<$10 nm, 10∼100 nm, 100∼1000 nm, and $>$1000 nm respectively (Hodot, 1961).

2. Experiments

2.1. Sampling and test for basic physical characteristics of coal samples

To reveal the differences in the PSD for different coal ranks based on different testing methods, four coal samples with different types of coal ranks from the Sihe (SH), Chengzhuang (CZ), Yuwu (YW), and Xinyuan (XY) coal mines of the SQB in China, were used for analysis in this study. The samples were tested for their basic characteristics, such as their $R_{o,\max}$ value, maceral composition, proximate analyses, and permeability, according to GB/T 6948-2008 (AQSIO, 2008a), GB/T8899-2013 (AQSIO, 2013), GB/T212-2008 (AQSIO, 2008b), and SY/T 6385-2016, respectively. Moreover, an AXIO Imager M1m Microspectrophotometer was used for measuring the coal petrography ($R_{o,\max}$ and maceral composition), and the test for the coal permeability was conducted with the steady state method under constant confining pressure according to the original stress of the coal seam (NEA, 2016). The collection of the coal samples adopted columnar sampling according to GB/T 475-2008, and the coal samples were pulverized to particles with a size range of 0.18∼0.25 mm for the determination of the $R_{o,\max}$ value, maceral composition, proximation, and MIP analysis, according to GB/T 16773-2008 (AQSIO, 2008c).

2.2. Test on the PSD of coal samples

A set of experiments, including MIP, LTNA, LFNMR, and NMRC methods, were conducted in series for each sample. MIP was applied using an Autopore IV 9500 (Micromeritics Instrument, USA) at a pressure of up to 60,000 psia (413.7 MPa), following ISO 15901-1-2016 (ISO, 2016), and its experimental course adopted constant pressure control. LTNA was conducted on an automated surface area and pore size analyzer, Tristar II 3020 (Micromeritics Instrument, USA), according to ISO 15901-2007 (ISO, 2007). Pulverized coal with a 45∼60 mesh particle size was used as the experimental sample in LTNA, and nitrogen was applied as the adsorbate under an analysis bath temperature of ∼195.85 °C. The N_2 data collected for the crushed sample were interpreted using multipoint BET analysis for the surface area and BJH analysis for the PSD (Gregg and Sing, 1982; Clarkson and Bustin, 1999; Clarkson et al., 2013).

LFNMR measurements are obtained using a MicroMR23-025V LFNMR analyzer (Niumag Corporation Ltd, China), which applied the relationship between the pore size and the condensation temperature of the fluid in the pores to estimate the PSD. The main preparation method of the coal samples for LFNMR includes mechanical crushing of the coal samples, generating block coal samples with a size range from 3∼5 cm, and saturating the coal samples in water under a vacuum pressure of 20 MPa for a 48 h period; the experimental principle and process were specified in a previous study (Yao and Liu, 2012). A schematic diagram of the LFNMR is shown in Fig. 1.

The main principle of LFNMR is described as follows. The spinning hydrogen nuclei in the fluid manifest NMR relaxation behavior under the combined action of a radio frequency field and a static magnetic field, which can be expressed as follows through T_2:

$$\frac{1}{T_2} = \frac{1}{T_{2B}} + \frac{1}{T_{2S}} + \frac{1}{T_{2D}} \tag{1}$$

where T_2 is the relaxation time of the fluid, with unit ms; T_{2B} is the body relaxation time, with unit ms; T_{2S} is the surface relaxation time, which is caused by the interaction between the fluid and the pore surface, with unit ms; and T_{2D} is the relaxation

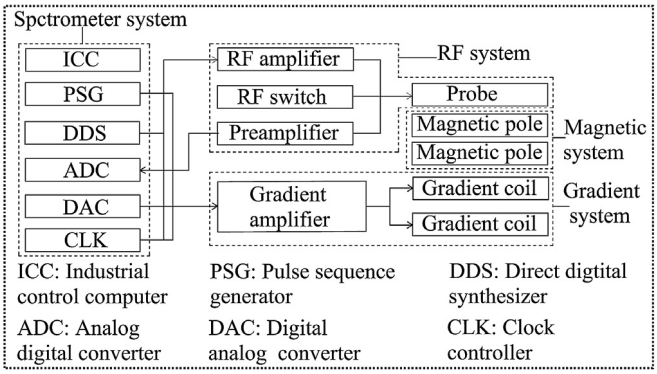

Fig. 1. Schematic diagram of LFNMR analyzer MicroMR 23-025V.

time caused by diffusion, with unit ms. In addition, when the magnetic field is the same (the corresponding magnetic intensities are extremely low) and the echo time is sufficiently short, T_{2D} can also be neglected. Here, T_2 can be expressed as follows:

$$\frac{1}{T_2} \approx \frac{1}{T_{2B}} = \rho\left(\frac{S}{V}\right) \tag{2}$$

where S is the surface area of the pores, cm^2; V is the pore volume, cm^3; and ρ is the transverse surface relaxation strength of the coal. Finally, the T_2 spectrogram can be converted into a diagram of the PSD by the linear conversion method (Wang et al., 2018).

NMRC measurements are obtained using Micro 12-010V-T NMRC analyzers (Niumag Corporation Ltd, China). The main preparation of the coal samples in the NMRC includes mechanical pulverization, generating coal particles with a 35∼50 mesh; the processing of the coal samples under a temperature of 373.15 K for a 24 h period; and the saturation of the coal samples in water. The experimental procedure and calibration of the NMRC are reported from a relevant study (Zhao et al., 2017). A schematic diagram of the NMRC is shown in Fig. 2. The NMRC can be used to directly obtain the pore volume from the linear relation between the pore volume and the signal intensity. The NMRC is applied to acquire the pore information from the melting process and is not influenced by the background signals. The detailed technical parameters and the detailed experimental parameters of the LFNMR and NMRC analyzers are listed in Table 1.

In addition, XRD was employed to analyze the content and types of minerals in the coal samples. Pulverized coal samples with a mesh size of <325 (0.045 mm) were applied for the XRD experiments. The observations and quantitative analyses of the pores and the minerals for all the coal samples were conducted on a ZEISS Sigma FE-SEM operating at 20 kV and equipped with an energy dispersive spectrometer for the analyses of the mineral composition, based on SY/T 5162-2014 and SY/T 6189-1996 (CNPC, 1996, 2014). The small coal pillars used for FE-SEM were polished using a cross-section polisher to grind off the oxide layer (approximately 1∼2 μm thick) of the coal pillars and were not spluttered with a gold coating or other materials.

3. Results and discussion

3.1. Basic characteristics of the coal sample

Table 2 shows the burial depth of the coal samples, as well as the permeability, maceral composition, coal quality, $R_{o,max}$ value, and bulk density. As shown in Table 2, the SH and CZ samples are anthracite, the YW sample is semianthracite, and the XY sample is low volatile bituminous coal. The coal permeability has a weak relation with the burial depth, and the maceral composition and is strongly associated with the coalification degree, mineral content, and A_{ad}. The coal permeability of the SH and CZ samples is clearly higher than that of the YW and XY samples, which is related to the coalification degree ($R_{o,max}$). However, the permeability of the SH sample is lower than that of the CZ sample, which is relevant to the mineral content and A_{ad}. The SH sample has the highest mineral content and A_{ad}; a higher mineral content may result in filling of the pores or fractures and may lead to a decrease in the permeability. Among all samples, the YW sample has the deepest burial depth, and its permeability is clearly lower than that of the SH and CZ samples. Table 3 shows the mineral composition of all the coal samples; as Table 3 indicates, the contents of the clay minerals from the SH, CZ, and XY samples are clearly higher than that of the YW sample. The filling amount of the clay minerals strongly affects the coal permeability, and among the selected coal samples, the XY sample has the highest content of clay minerals; therefore, its permeability is the lowest. In the anthracitic samples, the contents of the clay minerals of the SH sample are higher than those of the CZ sample, which results in a lower coal permeability of the SH sample than that of the CZ sample. For the semianthracitic and low volatile bituminous coal, the amount of clay mineral in the XY sample is higher than that of the YW sample, which leads to a higher permeability of the coal of the YW sample than that of the XY sample.

3.2. Genetic types of the pores in the coal samples

The genetic types of the pores in coal from the SQB were previously discussed (Bustin et al., 2008; Liu et al., 2017). Fig. 3 shows the pore types in the coal samples. Clay minerals such as kaolinite (Fig. 3a, b, g, j, k), dolomite (Fig. 3a, b, e, g), and illite (Fig. 3g and k) are widely developed, whereas calcite (Fig. 3e) and pyrite (Fig. 3j) are sporadically found in coal samples, filling in the protogenetic pores of the coal samples. The pore types in the coal samples mainly contain gas, intercrystal, and dissolved pores, the size of which varies from several to several hundred nanometers (Fig. 3c, f, i, l). The genetic types of pores in the coal samples suggest that the PSD of the coal samples is affected by the filling of the minerals.

3.3. Pore structure and its influence factor

3.3.1. PSD determined from MIP

The relationships of the cumulative pore volume with the intrusion pressure and the pore diameter in the coal sample plot using mercury intrusion and mercury extrusion are shown in Fig. 4, the pore volume and percentage of the different types of pores are indicated in Table 4, and the surface areas of the different types of pores are shown in Table 4.

As indicated in Fig. 4 and Table 4, the PSD suggests that there is significant substantial volume change in the transition pores to the micropores; the ratio of the macropores is approximately 10% with a low pore volume, and the ratio of the mesopores is lowest in terms of the pore volume among all the samples, whereas that of the micropores is the highest. The MIP suggests that there is a multimodality of the PSD for all the coal samples, and the peak values of the incremental pore volume correspond to pore diameter of approximately 10, 30, 80, and >1000 nm, meaning that the pore volumes experience a remarkable increase when the pore diameter is below 100 nm, which further suggests that the micropores develop well at a diameter of below 100 nm, and develop partial macrospores in the coal. A comparison between Fig. 4 and Table 4 indicates that the peak of the incremental pore volume at the pore diameter is consistent with the volume

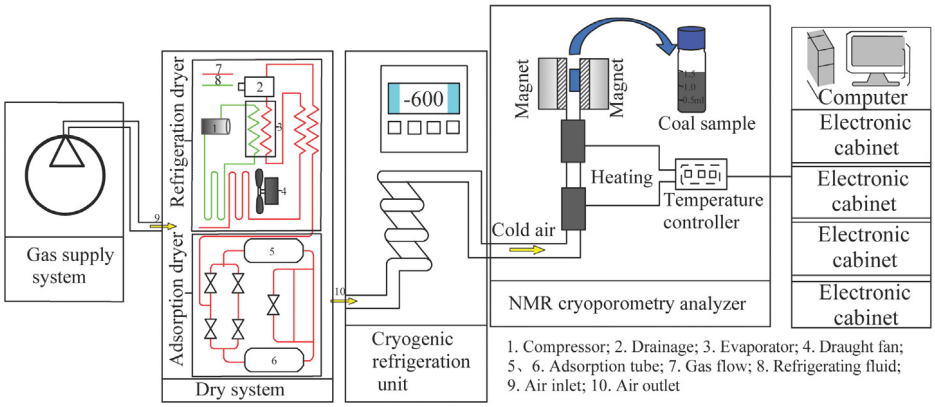

Fig. 2. Schematic diagram of NMRC pore analyzer Micro 12-010V-T.

Table 1
Specifications of LFNMR analyzer MicroMR23-025V and NMRC analyzer 12-010V-T.

Attribute	Parameter	
	LFNMR	NMRC
Magnet type	Permanent magnet	Permanent magnet
Magnetic field intensity (T)	0.055 ± 0.01	0.3 ± 0.05
Probe coil diameter (mm)	25	11
Temperature control range (°C)	−30 to 40	−30 to 40
Temperature control accuracy (°C)	35 ± 0.02	35 ± 0.02
Cooling rate (°C/min)	Average 1	Average 1
Sample volume (cm^3)	0.5–1	0.5–1
Aperture measurement effective range (nm)	10∼100,000	2–500
Echo time (ms)	0.16	0.1
90° pulse width (μs)	8	5
180° pulse width (μs)	15.6	10
Cumulative sampling number	32	256
Wait time (ms)	2000	500

Table 2
Characteristics for permeability, coal petrology, coal quality, and $R_{o,max}$, bulk density of coal samples.

Sample ID	Burial depth (m)	Permeability (mD)	Maceral composition (wt %)			Proximate (wt %)			$R_{o,max}$ (%)	Bulk density (g/cm^3)
			Vitrinite	Inertinite	Mineral	M_{ad}	A_{ad}	V_{daf}		
SH	326	0.064	68.61	15.78	15.61	1.48	13.12	6.32	3.33	1.30
CZ	457	0.077	72.22	20.39	7.39	2.71	12.18	6.94	2.96	1.26
YW	539	0.022	69.74	22.56	7.70	1.10	11.98	13.44	2.19	1.28
XY	400	0.013	74.93	17.84	7.23	0.81	5.35	15.26	1.81	1.19

Notes: wt %, weight percentage; M_{ad}, moisture content; A_{ad}, ash content; V_{daf}, volatile content.

Table 3
Miner types in coal samples of SH sample, CZ sample, YW sample, XY sample.

Sample ID	Miner type and its content (%)									
	Kaolinite	Illite	Chlorite	Feldspar	Calcite	Dolomite	Quartz	Rutile	Bauxite	Apatite
SH	15.73	52.35	0	7.42	11.27	1.55	11.68	0.00	0	0
CZ	30.06	30.17	0	26.07	3.21	2.71	2.78	1.02	3.98	0
YW	8.21	38.00	0	2.01	0.00	1.41	33.01	3.20	0	14.16
XY	73.27	5.42	0	8.00	2.61	4.23	6.47	0	0	0

fraction of the PSD, and when the pore diameter is lower than 100 nm, the volume fraction between the micropores and the transition pores has a remarkable ratio. However, when the curve of the mercury extrusion lags behind the curve of the mercury intrusion when the pore diameter is between 10 nm and 80 nm, the cumulative pore volume is almost invariable when the pore diameter is beyond 80 nm, which indicates that there may be abundant disconnected pores in the range of the transitional pores in the coal samples, The different coal samples have similar characteristics in terms of the multimodality of the PSD, but it can be seen that there is a difference in the peak amplitude of the incremental pore volume, which can be generated by the difference in the coal rank, maceral composition, and coal quality. Meanwhile, all the samples show the greatest pore volume and surface area within a pore size (diameter) of below 100 nm. The surface area from the transition pores and the micropores is dominant for all types of pores, which is consistent with the PSD.

Based on the results shown in Table 4, the XY sample has the highest total pore volume, the CZ sample has the highest porosity, the SH sample has the lowest total pore volume and porosity, and the YW sample has the lowest surface area. For the anthracitic samples, the total pore volume, porosity, and surface area of the CZ sample are all higher than those of the SH sample. This result is consistent with the coal permeability of the two samples, and further reveals the effects of the clay mineral content, which means that filling the clay minerals in the pores vastly affects the

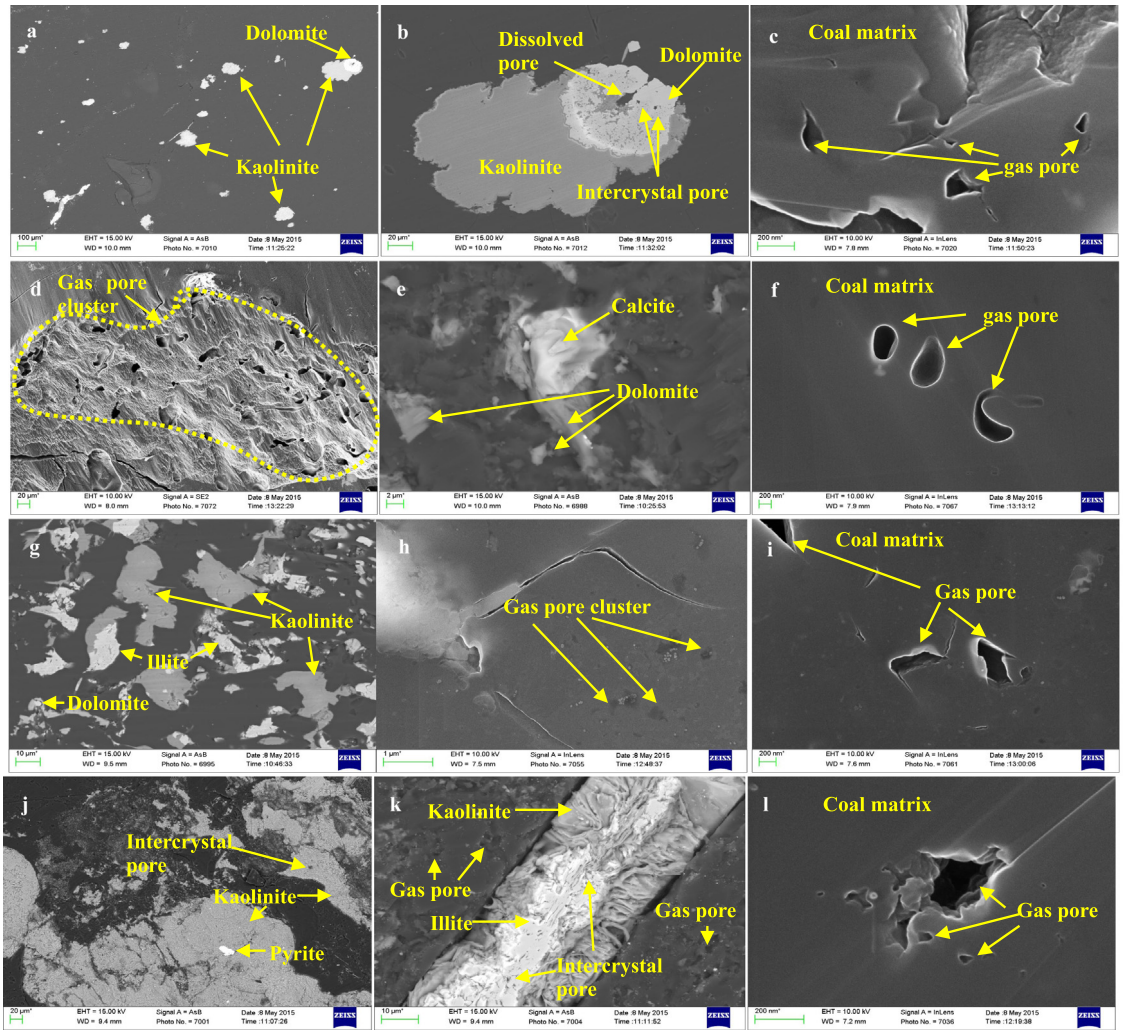

Fig. 3. Pore types and mineral composition in SH sample (a, b, c), CZ sample (d, e, f), YW sample (g, h, i), and XY sample (j, k, l) by FE-SEM.

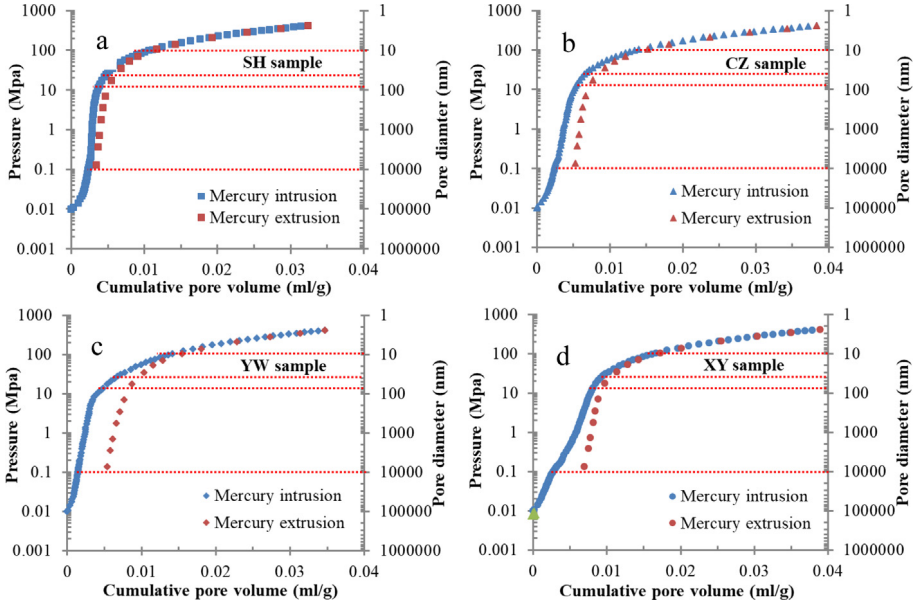

Fig. 4. Relationship of cumulative Hg pore volume with pressure and pore diameter in coal plots for SH sample (a), CZ sample (b), YW sample (c), and XY sample (d).

Table 4
Pore volume and its percent in different coal samples by MIP.

Sample	Pore volume (10^{-4} cm^3/g)					Volume fraction of PSD (%)				φ_{MIP} (%)
	V_1	V_2	V_3	V_4	V_t	V_1/V_t	V_2/V_t	V_3/V_t	V_4/V_t	
SH	29.18	9.28	86.12	200.02	324.60	8.99	2.86	26.53	61.62	4.22
CZ	37.49	16.45	101.50	228.36	383.80	9.77	4.28	26.45	59.50	4.84
YW	24.70	21.16	110.09	190.76	346.71	7.12	6.10	31.75	55.03	4.44
XY	60.48	20.05	100.70	207.08	389.03	15.55	5.15	25.87	53.23	4.65

Notes: V_1∼V_4, pore volume of macropore, mesopore, transition pore, and micropore respectively; V_t, total pore volume; V_1/V_t∼ V_4/V_t, means percentage from macropore, mesopore, transition pore, and micropore in the total pore volume respectively; φ_{MIP} means total porosity by MIP, %.

pore structure of the SH sample (Table 2). For the semianthracitic sample and the low volatile bituminous sample, the total pore volume, porosity, and surface area of the XY sample are all higher than those of the YW sample, which is consistent with the coal permeability of the two samples, and further reveals the effect from the content of the clay minerals; that is, the filling of the clay minerals in the pores substantially affects the pore structure of the XY sample (Table 2). As indicated in Table 2, the total pore volume of the coal sample is affected by the macropores and the mesopores, thereby directly affecting the porosity. Based on a comparison of the total pore volume with the porosity of all the samples, the total pore volume of the XY sample is the highest, followed by the CZ, YW, and SH samples; in addition, the sequence of the total pore volume is consistent with the total volume of the macropores and the mesopores, which results in a higher total pore volume of the XY sample than that of the CZ, YW, and SH samples. As shown in Table 4, the porosity of the CZ sample is the highest, followed by the XY, YW, and SH samples. This sequence of porosity is inconsistent with the sequence of the total pore volume for all the coal samples, which occurs because the porosity of a coal sample is related not only to its total pore volume, but also to its bulk density. As shown in Table 2, the sequence of the bulk density of all the samples is consistent with the porosity of all the samples, and the XY sample has the lowest bulk density and the largest volume of the coal matrix, which results in a decrease in the porosity. This result demonstrates why the XY sample has the largest total pore volume among all the samples, and why the porosity of the XY sample is lower than that of the CZ sample. Based on a comparison of the results from the total pore volume (Table 4) with the coal permeability (Table 2) of all the samples, it can be seen that the sequences of the total pore volume and the coal permeability of all the samples are inconsistent, which occurs because the coal permeability is related not only to the PSD but also to the connectivity of the pores of the coal sample.

A comparison shows that the SH sample has the lowest total pore volume and total surface area among all of the coal samples (Tables 4 and 5) and that the distribution of the total surface area is inconsistent with the total pore volume of all the samples; more specifically, the CZ sample has the highest pore volume of the micropores, followed by the XY, YW, and SH samples, whereas the CZ sample has the largest total surface area, followed by the XY, SH, and YW samples. However, the surfaces of all the coal samples show good consistency with the volume of the micropores for all the samples, which occurs because the total surface area of the coal sample is determined by the number of pores, and is particularly related to the number of micropores; the YW sample has a higher total pore volume and a lower total surface area than the SH sample, in which is because the SH sample having a higher pore volume and surface area of the micropores.

3.3.2. PSD determined from LTNA

As discussed in corresponding studies (Bustin et al., 2008; Clarkson et al., 2013), N_2 adsorption at ∼196 °C can be used to investigate the volume of the vast micropores to the transition pores. The adsorption curves from the SH, CZ, and XY samples are shown in Fig. 5. As Fig. 5 indicates, the CZ sample has the highest absorption, whereas the YW and SH samples have moderate adsorption, and the XY sample has the lowest absorption, which demonstrates that the pores in the CZ sample develop the best, the pores in the YW and SH samples develop relatively well, and the pores in the XY sample develop the worst. In addition, there is a wide hysteresis loop and an inflection point shown in the adsorption curve of the SH sample, and a relatively wide hysteresis loop and an inflection point in the adsorption curves of the CZ and YW samples, which indicate that the open pores develop the best in the SH sample; however, they develop well in the CZ and YW samples, but there is almost no hysteresis loop or inflection point in the XY sample, suggesting that there is an abundance of closed pores.

Plots of the cumulative and incremental pore volumes versus the pore size for nitrogen show the pore volume distributions (corresponding to the pore size) of the samples (Fig. 6).

As shown in Fig. 6a, when the pore diameter is less than approximately 20 nm, the cumulative pore volume of the SH sample is more than that of the CZ, YU, and XY samples, which indicates that the development of the micropores from the SH sample is superior to that of the CZ, YU, and XY samples. When the pore diameter is more than 20 nm, the cumulative pore volume of the CZ sample increases dramatically and is far greater that of the other coal samples. When the pore diameter is higher than approximately 30 nm, the cumulative pore volume of the YW sample exceeds that of the SH sample. Fig. 6a shows that the cumulative pore volume of the XY sample is always lower than that of the SH, CZ, and YW samples. The results indicate that the cumulative pore volumes of the SH and XY samples increase slowly from Fig. 6a, which may be related to the high content of minerals, such as clay and carbonate minerals (Tables 2 and 3). Most of the coal samples exhibit a remarkable cumulative pore volume when the pore diameter reaches 40 nm. As shown in Fig. 6b, a bimodality of the incremental pore volume (peaks at approximately 20 and 40 nm) and a trough in the incremental pore volume (trough at ∼30 nm) occur in the PSD for all the coal samples; the pore volume shows a remarkable increment within the pore diameter ranges of 0∼20 and 30∼40 nm, and when the pore diameter is beyond 40 nm, the incremental pore volume of all the samples drastically decreases. A quick decrease in the incremental pore volume from the transition pores with a pore diameter of 20∼30 nm and beyond 40 nm may be related to the growth of the transition pores and the filling of the minerals within the pores.

The pore volumes and BET surface areas obtained from the N_2 adsorption analysis are shown in Table 6. As indicated in Table 6, the CZ sample exhibits the highest total volume of the transition pores and micropores, whereas the XY sample exhibits the least total volume of the transition pores and micropores, the SH sample exhibits the highest BET surface area, and the XY sample demonstrates the smallest BET surface area. The total pore volume of a coal sample is mainly controlled by the ratio of the

Table 5
Surface area of pore with different pore diameter from coal samples by MIP.

Sample	Surface area (m^2/g)					Percentage of PSD on surface area (%)			
	S_1	S_2	S_3	S_4	S_t	S_1/S_t	S_2/S_t	S_3/S_t	S_4/S_t
SH	0.001	0.02	1.80	16.66	18.49	0.01	0.11	9.75	90.13
CZ	0.002	0.03	2.10	19.03	21.17	0.01	0.14	9.93	89.92
YW	0.002	0.05	2.11	15.72	17.87	0.011	0.26	11.79	87.94
XY	0.005	0.03	2.07	17.05	19.16	0.03	0.17	10.81	88.99

Notes: S_1∼S_4 means surface area of macropore, mesopore, transition pore, and micropore respectively; S_t, total pore volume; S_1/S_t∼S_4/S_t means percentage of surface area from macropore, mesopore, transition pore, and micropore in total surface area respectively.

Table 6
Pore volume and BET surface area of coal sample determined by LTNA.

Sample ID	Pore volume (10^{-4} cm^3/g)			Volume fraction of PSD (%)		BET surface (m^2/g)
	V_3	V_4	V_t	V_3/V_t	V_4/V_t	
SH	9.85	6.84	16.69	59.02	40.92	1.36
CZ	22.43	3.89	26.32	85.22	14.78	0.45
YW	15.60	3.78	19.38	80.49	19.51	0.48
XY	4.14	0.07	4.21	98.41	1.59	0.06

Notes: V_3∼V_4, transition pore, and micropore respectively; V_t, total pore volume; V_3/V_t∼ V_4/V_t means percentage from transition pore, and micropore in the total pore volume respectively.

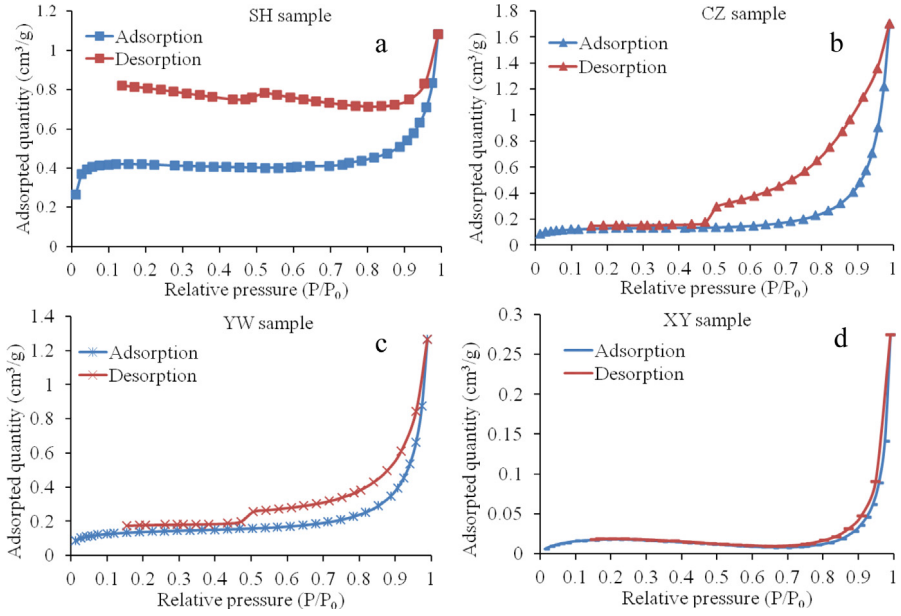

Fig. 5. N_2 adsorption isotherms for SH sample (a), CZ sample (b), YW sample (c), and XY sample (d).

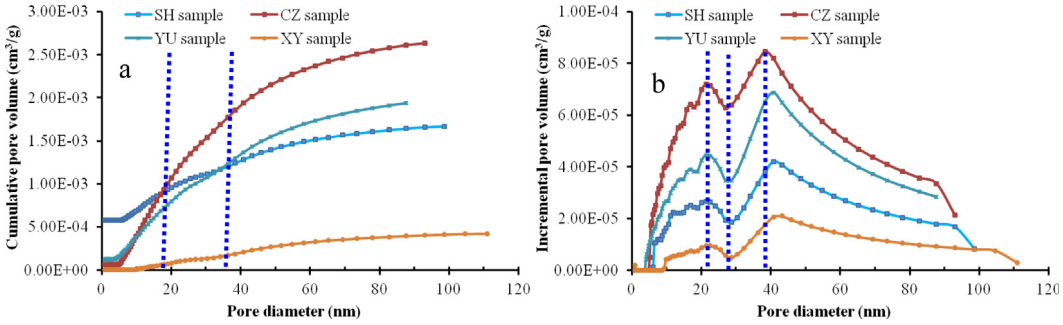

Fig. 6. Cumulative (a) and incremental (b) N_2 pore volume plots for SH sample, CZ sample, YW sample, and XY sample.

transition pores, that is, the volume of the transition pores is higher, and the total pore volume in the coal sample is higher. As a comparison between the total pore volume determined from MIP and the total pore volume determined from LTNA indicates, the distribution of the pore volume from the different pore diameters when using MIP is different from the distribution of the pore volume from the different pore diameters when using LTNA; that is, the total pore volume in a coal sample is controlled by the

volume of the transition pores and micropores when using MIP, and the total pore volume in the coal sample is controlled by the volume of the transition pores. It is worth mentioning that the XY sample has the highest total pore volume when using MIP, but has the lowest total pore volume when using LTNA, which may be related to the XY sample having the highest amount of clay minerals. The results when using LTNA shown in Table 6 indicate that the total pore volume from the anthracitic samples is higher than the total pore volumes from the semianthracitic sample and the low volatile bituminous sample, which suggests that the coalification degree ($R_{o,max}$) affects the PSD of the coal sample. The BET surface area of the coal sample is mainly determined by the micropores, that is, the ratio of the volume from the micropores to the total pore volume is high. Because the BET surface area of the coal sample is high, the growth of the micropores and the filling degree of the clay minerals affect the BET surface area of all the samples in the studied area. Through the integration with the above analysis and the results from Tables 2, 3, and 6 and Figs. 5 and 6, the effects of $R_{o,max}$, and the mineral content on the PSD of all the coal samples are clear.

3.3.3. PSD determined from LFNMR and NMRC

According to Eq. (2), T_2 spectral distributions can be converted into the PSD of the coal samples. Figs. 7 and 8 show the T_2 spectra distributions and PSD of all the coal samples when using the LFNMR, respectively. As shown in Figs. 7 and 8, with the T_2 distribution with the smallest pores having the shortest relaxation times and the largest pores having the longest relaxation times, the relaxation time is only 0.1 ms, which can be used to detect micropores with a pore diameter of 10 nm; however, the relaxation is only 0.9 ms, which can be used to detect transition pores with a pore diameter of approximately 10∼100 nm. The T_2 spectrum distribution of all samples (with two weak peaks shown in the enlarged section in Figs. 7 and 8), particularly the T_2 spectrum distribution of the YW and XY samples, present three clear peaks. The incremental pore volume of all the samples presents multimodality, with the three peaks representing the transition pores, macropores, and fracture. Among all of the samples, the matching diameters of the transition pores with the first peak of the incremental pore volume for the SH, CZ, YW, and XY samples are approximately 60, 40, 10, and 18 nm, respectively. As indicated in Fig. 8a and b, the porosity of all the samples is mainly due to the contribution of the transition pores, whereas the porosity of the mesopores and macropores from all the samples is extremely low; in particular, the porosity of the mesopores is the lowest for the all samples. When the pore diameter is greater than 1000 nm, the porosity from all the samples is mainly due to the contributions of the macropores and fractures. Through the comparisons, the cumulative porosity of the micropores from the SH and CZ samples is clearly lower than that of the YW and XY samples, and the cumulative porosity of the transition pores from the SH and CZ samples is obviously higher than that of the other samples (Fig. 8a). The incremental porosity of the micropores from the YW and XY samples is higher than that of the SH and CZ samples (Fig. 8b). A comparison of the results for the pore volume when using MIP, LTNA, and LFNMR shows that the ratio of the micropores from the SH and CZ samples is lower than that of the YW and XY samples when using LFNMR, which differs from the ratio of the micropores when using MIP and LTNA. This indicates that the SH and CZ samples mainly develop micropores with a smaller pore diameter, in contrast to the YW and XY samples. These micropores with a smaller pore diameter in the SH and CZ samples may be residual gas pores, and perhaps even gas pores filled with clay minerals, and are difficult to detect because of the relaxation time (T_2 time) of LFNMR.

The pore volume fraction was calculated according to the cumulative and incremental porosities, the results of which are

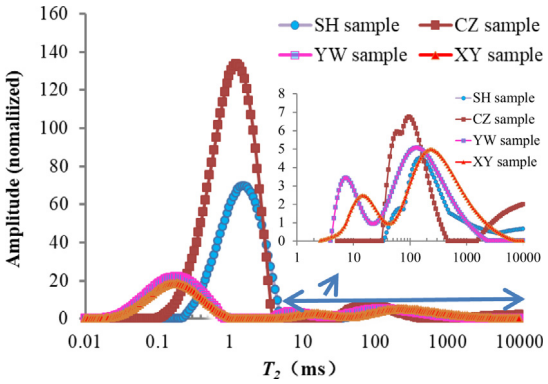

Fig. 7. LFNMR T_2 distribution at saturated water for SZ sample, CZ sample, YW sample, and XY sample.

Table 7
Porosity of different pore and volume fraction of selected coal samples tested by LFNMR.

Sample ID	Porosity (%)					Volume fraction of PSD (%)			
	φ_1	φ_2	φ_3	φ_4	φ_t	φ_1/φ_t	φ_2/φ_t	φ_3/φ_t	φ_4/φ_t
SH	0.70	1.49	7.05	0.01	9.25	7.57	16.11	76.21	0.11
CZ	0.51	0.61	8.00	0.27	9.39	5.43	6.50	86.49	2.88
YW	0.49	0.11	1.04	0.60	2.24	21.88	4.91	46.43	26.78
XY	0.66	0.03	1.25	0.30	2.24	29.46	1.34	55.81	13.39

Notes: φ_1∼φ_4, porosity of pore volume from macropore, mesopore, transition pore, and micropore respectively; φ_t, total porosity; φ_1/φ_t∼φ_4/φ_t means percentage from macropore, mesopore, transition pore, and micropore in the total pore volume respectively.

shown in Table 7. As indicated in Table 7, there is an obvious difference in the porosity and volume fraction among each of the samples. The SH and CZ samples show a higher total porosity and in particular have a high porosity of the transition pores, in contrast to the YW and XY samples. The YW and XY samples have a higher porosity of the micropores, in contrast to the SH and CZ samples. Matching the porosities, the volume fraction of the transition pores from the SH and CZ samples is higher than that of the YW and XY samples, and the volume fraction of the micropores from the YW and XY samples is higher than that of the SH and CZ samples. Comparing Fig. 8 and Table 7, the pore diameter associated with the first peak from the transition pores is 10∼60 nm; in addition, the transition pores have an advantage in the volume fraction of the PSD for all the samples, although the micropores have a higher proportion in the semianthracitic sample and low volatile bituminous sample. The location where the first peak of the incremental porosity occurs at the pore diameter is consistent with the volume fraction of the transition pores.

Integrating Tables 2, 3, and 7, and Fig. 8, there is a clear control from $R_{o,max}$ in the coal reservoir, and the total porosity of the anthracitic samples is higher than that of the semianthracite coal samples and higher than that of the low volatile bituminous coal; therefore, the total porosity of the SH and CZ samples is higher than that of the semianthracite coal sample, such as the YW sample and is higher than that of the low volatile bituminous coal sample, such as the XY sample. Second, the mineral content and burial depth of the coal both have a remarkable effect on the total porosity of the coal samples; in addition, the SH sample has a high mineral content, leading to a total porosity below that of the CZ sample, whereas the YW sample has the deepest burial depth, which leads to a total porosity equal to that of the XY sample.

Cumulative and incremental intrusion plots using the NMRC are shown in Fig. 9. As indicated in Fig. 9, there are relatively

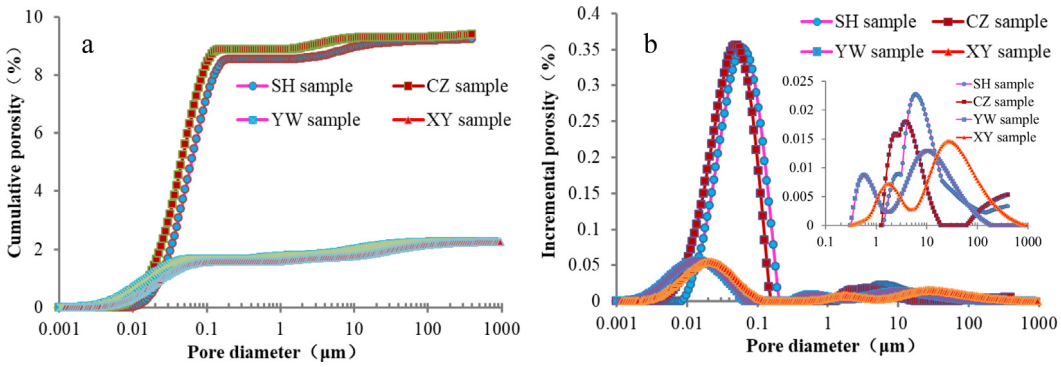

Fig. 8. LFNMR PSD curves at saturated water for SZ sample, CZ sample, YW sample, and XY sample (a: cumulative porosity; b: incremental porosity).

clear differences in the cumulative and incremental pore volumes among all the samples. As shown in Fig. 9, the SH, CZ, and XY samples have a high cumulative pore volume, whereas the YW coal sample has a relatively low cumulative pore volume. It is easy to see that the cumulative pore volumes of the XY and SH samples are higher than those of the CZ and YW samples. The results from NMRC are different from those of MIP, LTNA, and LFNMR, which occurs because NMRC can detect not only the interconnected pores but also the disconnected pores. According to Tables 2 and 3, the total amounts of clay minerals, calcite, and dolomite in the SH, CZ, YW, and XY samples are 80.90%, 66.15%, 47.62%, and 85.53%, respectively, which suggests that a number of disconnected pores may occur in the SH, CZ, and XY samples; in addition, the amount of disconnected pores from the XY sample is the highest, followed by the SH and CZ samples, which is in accordance with the analysis results from Fig. 5. Meanwhile, the cumulative pore volume from NMRC has a high negative correlation with the burial depth of the coal samples, and the compaction of the burial depth on the coal seam results in the pores closing. Among the coal samples, the burial depth of the YW sample is the deepest, and the compaction of the burial depth on the YW sample is the most significant; therefore, the cumulative pore volume of the YW samples is the lowest.

According to Fig. 9b, the incremental pore volume shows multimodality, and the incremental pore volume reaches a peak at the different pore diameters. The incremental pore volume of the SH sample shows a short peak at a pore diameter of approximately 2 nm, a relatively obvious peak at a pore diameter of 10 nm, and an obvious peak at a pore diameter of 30 nm, whereas the incremental pore volume of the CZ shows three main peaks at pore diameters of approximately 3, 10, and 60 nm. The incremental pore volume of the YW sample shows peaks at pore diameters of 2, 4, 6, 10, 20, and 60 nm. The incremental pore volume of the XY sample shows peaks at pore diameters of approximately 2, 30, and 100 nm. The incremental pore volume reaches a maximum at a pore diameter of 30 nm for the SH and XY samples, whereas the incremental pore volume reaches a maximum at a pore diameter of 60 nm for the CZ and YW samples. Comparing the cumulative and incremental pore volumes, all samples have a relatively high pore volume when the pore diameter is between 20 and 30 nm. As seen from Fig. 9b, when the pore diameter is lower than 30 nm, the incremental pore volume of the XY sample has the fastest growth, which is far higher than the incremental pore volume of the SH, CZ, and YW samples, indicating that the development of the disconnected pores with pore diameters below 30 nm in the XY sample is far better than that of the other coal samples. When the pore diameter is beyond 30 nm, the incremental pore volumes of the XY and SH samples show a downward trend overall, and the incremental pore volumes of the CZ and SH samples are higher than those of the XY and YW samples, which demonstrates that the development of the disconnected pores with pore diameters greater than 30 nm in the CZ and SH samples is better than that of the XY and YW samples.

Table 8 shows the pore volume fraction of the PSD for all samples according to the statistical results of NMRC. As shown in Table 8, the volume fraction of micropores and transition pores from all the samples is 77.80%∼90.77%, the volume fraction of the micropores is slightly more than that of the transition pores, and the volume fraction of the mesopores is the lowest. The volume fraction of the mesopores from the SH, CZ, YW samples is approximately 20%, which is approximately 10% higher than that of the XY sample. Integrating the results shown in Tables 2, 3, and 8, and Fig. 8, an obvious effect from the $R_{o,max}$, mineral content, and burial depth on the generation of pores in the coal reservoir is shown, all of which are factors that affect the pores; in addition, the burial depth of the coal samples has remarkable control over the pores of the coal samples.

3.4. Comprehensive analysis of the PSD based on MIP, LTNA, LFNMR, and NMRC

As discussed above, the pore volume, porosity, and surface area differ based on the different testing methods applied, and the differences in the pore volume, porosity, and surface are caused by the difference in the testing principle and the assumed theory models of the different testing methods. MIP is effective at analyzing the mesopores and macropores of coal samples but has difficulty distinguishing the transition pores and micropores of coal samples. LTNA is effective at analyzing the transition pores and micropores of coal samples but is unable to analyze the mesopores and macropores of coal samples. Moreover, the destruction of the pore structure occurs under high pressure when using MIP and LTNA, especially for MIP. LFNMR is effective at analyzing pores with a wide pore diameter. NMRC is effective at analyzing pore sizes from micropores to mesopores. MIP, LTNA, and LFNMR can detect the connected pores; in contrast, MIP and LTNA have difficulty detecting poorly interconnected pores, whereas LFNMR does not, and NMRC can detect not only interconnected pores but also disconnected pores.

As indicated in Figs. 4–9, MIP suggests a multimodality for all coal samples (peaks at pore diameters of approximately 10, 30, 80, and >1000 nm), LTNA suggests a bimodality for all coal samples with peaks at pore diameters of approximately 20 and 40 nm, LFNMR suggests a multimodality for all coal samples with peaks at pore diameters of approximately 10 and 20 nm, and NMRC suggests a multimodality for all coal samples with peaks at pore diameters of approximately 30 and 60 nm. The peak representation in the micropores and transition pores when using MIP is generally consistent with that of LTNA, LFNMR, and NMRC,

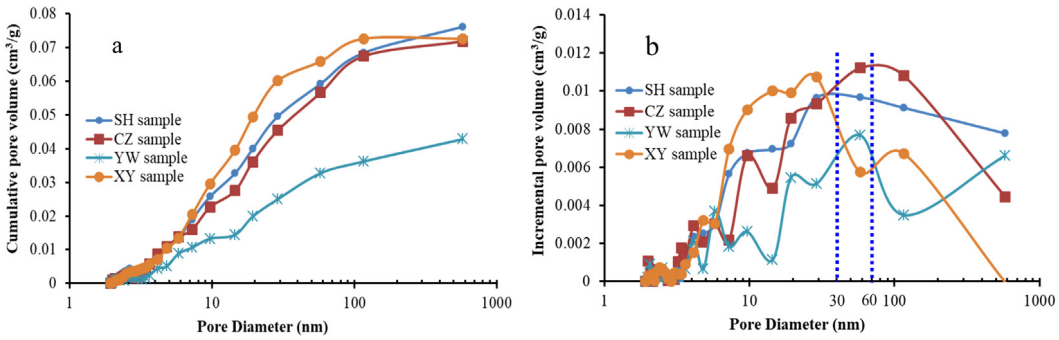

Fig. 9. Cumulative (a) and incremental (b) NMRC pore volume plots for SH sample, CZ sample, ZZ sample, YW sample, BF sample, and XY sample.

Table 8
Pore volume and volume fraction of different coal samples tested by NMRC.

Sample ID	Pore volume (10^{-4} cm^3/g)				Volume fraction of PSD (%)		
	V_2	V_3	V_4	V_t	V_2/V_t	V_3/V_t	V_4/V_t
SH	168.96	334.91	257.41	761.28	22.20	43.99	33.81
CZ	152.57	339.76	225.94	718.27	21.24	47.30	31.46
YW	101.16	194.15	132.79	428.10	23.63	45.35	31.02
XY	66.88	363.98	294.62	725.48	9.22	50.17	40.61

Notes: V_2∼V_4, mesopore, transition pore, and micropore respectively; V_t, total pore volume; V_2/V_t∼V_4/V_t means percentage from mesopore, transition pore, and micropore in the total pore volume respectively.

whereas the peak representation in the macropores when using MIP is consistent with that of LFNMR. As shown in Tables 4, 6, and 7, the pore volume fraction from the micropores and transition pores are consistent when applying MIP, LNTA, and LFNMR, which is not different from that of NMRC (Table 8), in which the pore volume fraction from the micropores and transition pores is approximately 80% except for that of the XY sample; in particular, the pore volume fraction of the transition pores shows the highest percentage in all types of pores from most of the samples. To compare the differences from the results of the analysis methods, the SH sample is chosen as an example, and the synthetic results are as shown in Table 9, based on the results in Figs. 4–9, and Tables 4, 6, 7, and 8.

Table 9 clearly shows the differences among the ranges of the pore diameters, the dominant pore diameter of the pore volume, and the volume fraction of the PSD for the SH sample. As shown in Table 9, MIP and LFNMR can detect all interconnected pores with different pore diameters, although the volume fraction of the micropores from LFNMR is clearly lower than that of MIP, which occurs because of the difficulty in testing the micropores owing to the short echo time when using LFNMR. As a nondestructive testing method, LFNMR can detect not only the connected pores but also poorly connected pores, and as a result, the volume fraction of the mesopores and the transition pores when using LFNMR is higher than those when using MIP. The volume fraction of the transition pores when using LTNA is clearly higher than that when using MIP. Mercury has difficulty entering disconnected and poorly connected mesopores and transition pores, and some information from these pores is difficult to obtain through the use of MIP. Based on a comparison with MIP, nitrogen easily flows in poorly connected mesopores and transition pores, and the volume fraction from the mesopores and transition pores is high. Owing to the occurrence of the remarkably disconnected pores, this leads to a high volume fraction of the transition pores when using NMRC compared with MIP. Furthermore, the volume fractions of the mesopores and transition pores when using NMRC are higher than those of MIP, which indicates that there is an abundance of disconnected pores in coal as revealed using NMRC. Based on the above analysis, there are remarkably poorly connected and disconnected mesopores and transition pores in the SH sample.

As indicated above, the pore volume in coal is mainly from the contribution of the transition pores and micropores based on the difference in the PSD from the different coal samples when tested using MIP, LTNA, LFNMR, and NMRC; the comparison results of the transition pores and micropores of the PSD based on the different analysis methods are shown in Table 10. As shown in Table 10, there are clear differences in the total pore volume of the transition pores and micropores when using MIP, LTNA, LFNMR, and NMRC, as discussed above, which is due to the differences in the analysis principles and the calculation models from the different analysis methods. There is no reason to compare the total pore volume from the different analysis methods. There is an obvious difference between the different coal samples in the total pore volume when applying MIP, as analyzed in Sections 3.3.1 through 3.3.3, and the difference in the pore volume between the different coal samples is controlled by $R_{o,max}$, the mineral content in the coal, and the burial depth of the coal sample. The SH sample has a relatively low pore volume when using MIP and LTNA, which suggests that a remarkable transition pores change into micropores with poor connectivity in coal owing to the filling of the minerals. Integrating the results of the total pore volume or total porosity when using MIP, LTNA, LFNMR, and NMRC, the differences in the different coal samples in the transition pores and the micropores are mainly controlled by $R_{o,max}$ and the burial depth of the coal samples. Meanwhile, the ratios of the transition pores in the summation of the transition pores and micropores when using LFNMR are higher than those when using LTNA and MIP, which is related to the destruction of the micropores when applying MIP and LTNA under high pressure, particularly for MIP. The pore fraction of the micropores when using NMRC is clearly higher than that when using LTNA and LFNMR, which suggests that remarkably disconnected micropores develop in the coal samples. A comparison of Tables 2 and 10 shows that the permeability of the coal samples is basically consistent with the total porosity or pore volume, particularly based on the results from LFNMR.

Based on the above analysis, affected by the connected macropores and mesopores, the XY and CZ samples show a high pore volume and porosity when using MIP (Table 4), whereas affected by the total pore volume and the bulk density (Tables 2 and 5),

Table 9
Comparison of PSD using by different analysis method from SH sample.

Analysis method	Pore diameter range (nm)	Dominant pore diameter of pore volume (nm)	Volume fraction of PSD (%)			
			Macropore	Mesopore	Transition pore	Micropore
MIP	>7.2	<100; >1000	8.99	2.86	26.53	61.62
LTNA	<100	2∼60			58.99	41.01
LFNMR	10∼100,000	10∼60; >1000	7.57	16.11	76.21	0.11
NMRC	2∼580	30∼60		22.20	43.99	33.81

Table 10
Comparison of PSD for different samples using by different analysis methods.

Sample	MIP			LTNA			LFNMR			NMRC		
	V_{3+4}	V_3/V_{3+4}	V_4/V_{3+4}	V_{3+4}	V_3/V_{3+4}	V_4/V_{3+4}	φ_{3+4}	φ_3/φ_{3+4}	φ_4/φ_{3+4}	V_{3+4}	V_3/V_{3+4}	V_4/V_{3+4}
SH	286.14	30.10	69.90	16.69	59.02	40.92	7.06	99.86	0.14	592.32	56.54	43.46
CZ	329.86	30.77	69.23	26.32	85.22	14.78	8.27	96.74	3.26	565.70	60.06	39.94
YW	300.86	36.59	63.41	19.38	80.49	19.51	1.64	63.41	36.59	326.94	59.38	40.62
XY	307.78	32.72	67.28	4.21	98.41	1.59	1.55	78.62	21.38	658.60	55.27	44.73

Notes: V_{3+4}, total pore volume of transition pore and micropore, 10^{-4} Ml/g; V_3/V_{3+4}∼V_4/V_{3+4}, means percentage from transition pore, and micropore in the total pore volume of transition pore and micropore respectively, %; φ_{3+4}, total porosity of transition pore and micropore, %; φ_3/φ_{3+4}∼φ_4/φ_{3+4}, means percentage from transition pore, and micropore in the total pore volume of transition pore and micropore respectively, %.

the CZ sample shows the highest surface area of the pores, the XY shows a relatively high surface area of the pores, the YW sample has the lowest surface area of the pores when using MIP. In addition, the PSD in the coal samples when using MIP is controlled by $R_{o,\max}$ and the coal quality, which is particularly based on the content of the clay minerals. Affected by the transition pores, the CZ sample shows the highest pore volume, the SH and YW samples show a relatively high pore volume, and the XY sample shows a low pore volume when using LTNA, which is controlled by the contents of the minerals such as clay minerals, calcite, and $R_{o,\max}$; in addition, the BET surface area when using LTNA shows good consistency with the volume of the micropores from all the samples. The SH and CZ samples have a higher volume fraction of the transition pores than the YW and XY samples and have a lower volume fraction of the micropores than the YW and XY samples when using LFNMR, which is affected by the growth of the micropores with a smaller pore diameter and is difficult to detect using LFNMR. Affected by the disconnected pores, the SH, CZ, and XY samples have a relatively high pore volume, and the YW sample has the lowest pore volume, when using NMRC. According to the comprehensive analysis described above, the PSD of anthracite is better than that of semianthracite, as well as that of the low volatile bituminous coal, for all coal samples selected; in addition, the SH and CZ samples develop better interconnected pores and worse disconnected pores, respectively, whereas the XY sample develops better disconnected pores. Moreover, the differences in the PSD for all the coal samples are comprehensively controlled by $R_{o,\max}$, the mineral content in the coal, and the burial depth of the coal sample.

4. Conclusions

Based on a synergetic analysis of the PSD of coal reservoirs from the SQB, China, using by MIP, LTNA, LFNMR, and NMRC, and comprehensively disclosing the reason for the difference in the PSD, the main conclusions were acquired as follows:

(1) Multimodality from all the samples occurs when using MIP, and anthracite coal has a higher pore volume, porosity, and surface area than semianthracite and low volatile bituminous coal. Affected by the total pore volume and the bulk density, the surface area of the pores in the coal is irrelevant to the types of coal.

(2) Most of the coal samples show the greatest amount of pore volume when using LTNA once the pore diameter reaches 40 nm, and a bimodality is shown in all the samples; the total pore volume is mainly derived from the contribution of the transitional pores. The growth of the micropores and the filling degree of the clay minerals affect the BET surface area of all the samples. Moreover, for the cumulative pore volume, the BET surface area from the anthracitic samples is basically higher than that of the semianthracitic and low volatile bituminous samples, which is affected by the filling of the minerals.

(3) The total porosity of all the samples when using LFNMR is mainly from the contribution of the interconnected pores including the transition pores and the micropores, and the total porosities of the mesopores and the macropores from all the samples are extremely low; in particular, the porosity of the mesopores is the lowest for all the samples. Anthracite has a higher total porosity than semianthracite coal and a lower total porosity than volatile bituminous coal. Anthracite coal develops micropores with a smaller pore diameter than semianthracite, and a low volatile bituminous coal develops. Such pores are difficult to detect owing to the value of T_2 of LFNMR.

(4) Differences in the cumulative and incremental pore volumes when using NMRC occur, and the total pore volume is mainly due to the contribution of the transition pores and micropores. The incremental pore volume shows a multimodality, and the incremental pore volume reaches a high peak value at different pore diameters. Numerous disconnected pores develop in all coal the samples, and the number of disconnected pores from the low volatile bituminous coal is the highest, followed by anthracite and semianthracite coal.

(5) Owing to the differences in the analysis principles and the calculation models from the different analysis methods applied, there are clear differences in the total pore volume of the transition pores and micropores when using MIP, LTNA, LFNMR, and NMRC. Regarding the poorly connected micropores in all the coal samples, the connectivity of the micropores in the anthracite coal is better than that in the semianthracite and low volatile bituminous coal samples; moreover, the difference in the PSD from the different coal samples based on the different analysis methods is comprehensively controlled through $R_{o,\max}$, the mineral content in the coal, and the burial depth of the coal samples.

Affected by the comprehensive factors, the permeability of the coal samples shows good consistency with the PSD.

Declaration of competing interest

The authors declare that they have no known competing financial interests or personal relationships that could have appeared to influence the work reported in this paper.

Acknowledgments

This study was supported by the University Natural Science Research Project of Anhui Province (KJ2019A0100), the National Natural Science Foundation of China (Grant Nos. 41727801, 41302129), the Anhui Provincial Natural Science Foundation (2008085MD121), and the Anhui postdoctoral research project (2017B171).

References

AQSIO, S.A.C., 2008a. GB/T6948-2008 Method of Determining Microscopically the Reflectance of Vitrinite in Coal. Standards Press of China, Beijing.

AQSIO, S.A.C., 2008b. GB/T 212-2008 Proximate Analysis of Coal. Standards Press of China, Beijing.

AQSIO, S.A.C., 2008c. GB/T 16773-2008 Method of Preparing Coal Samples for the Coal Petrographic Analysis. Standards Press of China, Beijing.

AQSIO, S.A.C., 2013. GB/T 8899–2013 Determination of Maceral Group Composition and Minerals in Coal. Standards Press of China, Beijing.

Bustin, R.M., Bustin, A.M.M., Cui, X., Ross, D.J.K., 2008. Impact of shale properties on pore structure and storage characteristics. In: 2008 SPE Shale Gas Production Conference. Fort Worth, Texas. SPE 119892. 16–18 November.

Clarkson, C.R., Bustin, R.M., 1999. The effect of pore structure and gas pressure upon the transport properties of coal: a laboratory and modeling study. 1. Isotherms and pore volume distributions. Fuel 78, 1333–1344.

Clarkson, C.R, Jensen, J.L., Blasingame, T.A., 2011. Reservoir engineering for unconventional gas reservoirs: what do we have to consider? In: SPE North American Unconventional Gas Conference and Exhibition. Woodlands, Texas. SPE 145080. 12–16 June.

Clarkson, C.R., Solano, N., Bustin, R.M., Bustin, A.M.M., Chalmers, G.R.L., He, L., Melnichenko, Y.B., Radliński, A.P., Blach, T.P., 2013. Pore structure characterization of North American shale gas reservoirs using USANS/SANS, gas adsorption, and mercury intrusion. Fuel 103, 606–616.

CNPC, 1996. SY/T 6189–1996. In: Quantitative Analysis Method of Rock Mineral By Energy Dispersive Spectrometry (EDS) in SEM. Standards Press of China, Beijing.

CNPC, 2014. SY/T 5162–2014. In: Analytical Method of Rock Sample By Scanning Electron Microscope. Standards Press of China, Beijing.

Fu, H.J., Tang, D.Z., Xu, T., Tan, S., Yin, Z.Y., Chen, B.L., Zhang, C., Wang, L.L., 2017. Characteristics of pore structure and fractural dimension of low-rank coal: A case study of Lower Jurassic Xishayao coal in the southern Junggar Basin, NW China. Fuel 193, 254–264.

Gane, P.A.C., Ridgway, C.J., Lehtinen, E., Valiullin, R., Furo, I., Schoelkopt, J., Paulapuro, H., Daicic, J., 2004. Comparison of NMR cryoporometry, mercury intrusion porosimetry, and DSC thermoporosimetry in characterizing pore size distributions of compressed finely ground calcium carbonate structures. Ind. Eng. Chem. Res. 43 (24), 7920–7927.

Gregg, S.J., Sing, K.S.W., 1982. Adsorption, Surface Area, and Porosity, second ed. Academic Press, New York.

Hodot, B.B., 1961. Outburst of Coal and Coalbed Gas (Chinese Translation). Industry Press, Beijing.

ISO, 2007. 15901-2007. In: Pore Size Distribution and Porosity of Solid Materials By Mercury Porosimetry and Gas Adsorption. ISO Copyright Office, Geneva.

ISO, 2016. 15901-1-2016. In: Evaluation of Pore Size Distribution and Porosity of Solid Materials By Mercury Porosimetry and Gas Adsorption—Part 1: Mercury Porosimetry. ISO Copyright Office, Geneva.

Jackson, C.L., McKenna, G.B., 1990. The melting behavior of organic materials confined in porous solids. J. Chem. Phys. 93 (12), 9002–9011.

Kondrashova, D., Valiullin, R., 2013. Improving structural analysis of disordered mesoporous materials using NMR cryoporometry. Micropor. Mesopor. Mat. 178, 15–19.

Li, Y., Zhang, C.M., Tang, D.Z., Gan, Q., 2017. Coal pore size distributions controlled by the coalification process: An experimental study of coals from the Junggar, Ordos and Qinhsui basins in China. Fuel 206, 352–363.

Liu, S.Q., Sang, S.X., Wang, G., Ma, J.S., Wang, X., Wang, W.F., Du, Y., Wang, T., 2017. FIB-SEM and X-ray CT characterization of interconnected pores in high-rank coal formed from regional metamorphism. J. Nat. Gas Sci. Eng. 148, 21–31.

Liu, H.H., Sang, S.X., Xue, J.H., Lan, T.H., Xu, H.J., Ren, B., Cheng, Q., 2018. Experimental study on the velocity sensitivity of coal reservoir during coalbed methane drainage in southern Qinshui Basin. Energy Explor. Exploit. 36 (6), 1593–1608.

Luo, C.J., Zhang, D.F., Lun, Z.M., Zhao, C.P., Wang, H.T., Pan, Z.J., Li, Y.H., Zhang, J., Jia, S.Q., 2019. Displacement behaviors of adsorbed coalbed methane on coals by injection of SO_2/CO_2 binary mixture. Fuel 247, 356–367.

Mastalerz, M., Drobniak, A., Strąpoc', D., Acosta, W.S., Ruppa, J., 2008. Variations in pore characteristics in high volatile bituminous coals: implications for coalbed gas content. Int. J. Coal Geol. 76, 205–216.

Mitchell, J., Webber, J., Strange, J., 2008. Nuclear magnetic resonance cryoporometry. Phys. Rep. 46, 1–36.

NEA, 2016. GB/T6948-2008 Porosity and Permeability Measurement under Overburden Pressure. Natural Energy Administration of China, Beijing.

Petrov, O.V., Furo, I., 2009. NMR cryoporometry: Principles, applications and potential. Prog. Nucl. Magn. Reson. Spectrosc. 54 (2), 97–122.

Petrov, O.V., Furo, I., 2010. A joint use of melting and freezing data in NMR cryoporometry. Micropor. Mesopor. Mat. 136, 83–91.

Shao, P., Wang, X., Song, Y., Li, Y., 2018. Study on the characteristics of matrix compressibility and its influence factors for different rank coals. J. Nat. Gas Sci. Eng. 56, 93–106.

Song, Y., Ma, X.Z., Liu, S.B., Jiang, L., Hong, F., Qin, Y., 2018. Accumulation conditions and key technologies for exploration and development of Qinshui coalbed methane field. Petrol. Res. 3, 320–335.

Wang, B., Sun, F.J., Tang, D.Z., Zhao, Y., Song, Z.H., Tao, Y., 2015. Hydrological control rule on coalbed methane enrichment and high yield in FZ Block of Qinshui Basin. Fuel 140, 568–577.

Wang, A.M., Wei, Y.C., Yuan, Y., Li, C.F., Li, Y., Cao, D.Y., 2017. Coalbed methane reservoir's pore-structure characterization of different macrolithotypes in the southern Junggar Basin of Northwest China. Mar. Pet. Geol. 86, 675–688.

Wang, F.Y., Yang, K., Cai, J.C., 2018. Fractal characterization of tight oil reservoir pore structure using nuclear magnetic resonance and mercury intrusion porosimetry. Fractals 26 (2), 1840006.

Xu, X.K., Meng, Z.P., Wang, Y., 2019. Experimental comparisons of multiscale pore structures between primary and disturbed coals and their efforts on adsorption and seepage of coalbed methane. J. Nat. Gas Sci. Eng. 174, 704–715.

Yao, Y.B., Liu, D.M., 2012. Comparison of low-field NMR and mercury intrusion porosimetry in characterizing pore size distributions of coals. Fuel 95, 152–158.

Yao, Y.B., Liu, D.M., Chen, Y., et al., 2010. Petrophysical characterization of coals by low-field nuclear magnetic resonance (NMR). Fuel 89, 1371–1380.

Zhang, M., Fu, X.H., 2018. Characterization of pore structure and its impact on methane adsorption capacity for semi-anthracite in Shizhuangnan Block, Qinshui Basin. J. Nat. Gas Sci. Eng. 60, 49–52.

Zhang, Z., Qin, Y., Zhuang, X.G., Li, G.Q., Wang, X.M., 2018. Poroperm characteristics of high-rank coals from southern Qinshui Basin by mercury intrusion, SEM-EDS, nuclear magnetic resonance and relative permeability analysis. J. Nat. Gas Sci. Eng. 51, 116–128.

Zhao, Y.X., Sun, Y.F., Liu, S.M., Wang, K., Jiang, Y.D., 2017. Pore structure characterization of coal by NMR cryoporometry. Fuel 190, 359–369.